Supporting Information

Excellent comprehensive electrical properties in KNN-based ceramics via synergistic effects of structural flexibility and domain engineering

Hongjiang Li[1], Ning Chen[1], Jie Xing[1], Hao Chen[1], Zhi Tan[1, *], Mingyue Mo[1], Qifan Chen[1], Jianguo Zhu[1, *], Feng Li[2], Zhenlong Liu[2], Weifeng Ouyang[2] and Huixiang Zhu[2]

[1] College of Materials Science and Engineering, Sichuan University, Chengdu, Sichuan, 610064, China.

[2] Guangzhou Kailitech Electronics Co., Ltd, Guangzhou, Guangdong, 511356, China.

Experimental section

$0.957(K_{0.48}Na_{0.52})Nb_{0.95}Ta_{0.06}O_3$-$0.04(Bi_{0.5}Na_{0.5})ZrO_3$-$0.003BiFeO_3$ + x LiF (KNNT-BNZ-BFO/x LiF) ceramics are produced by conventional roll forming technology. Firstly, the analytical grade reagents of high-purity raw materials are mixed by ball milling in a zirconia ball media and anhydrous ethanol solution for 15 to 20 h. Then, the powders are calcined at 800 to 950 °C for 6 h. The powders are re-milled with zirconia ball media and anhydrous ethanol solution for 15 to 20 h. The powders are milled with polyvinyl alcohol (PVA) colloid in a specific mass ratio (*e.g.* 100 g powder corresponds to 6 g PVA). The PVA-mixed powders are pressed into plates with a diameter of 14-15 mm and a thickness of 0.18-0.20 mm using the roll-forming process. Finally, the PVA is burnt off totally at 500 to 550 °C for 3 h, and then the samples are sintered in air at 1090 to 1105 °C for 3 to 5 h. The top and bottom surfaces of the samples are coated with 5 to 15 % weight of silver paste and then fired at 700 to 750 °C for 10 min to form electrodes for the measurement of electrical properties. The

* Corresponding author:
E-mail address: tanzhi0838@scu.edu.cn (Z. Tan), nic0400@scu.edu.cn (J. Zhu)

KNNT-BNZ-BFO/*x* LiF ceramics are processed in a silicon oil bath at 30 to 120 °C by applying a direct current (DC) electric field of 2 to 3 kV/mm for 15 to 20 min.

The crystal structure and phase purity of the ceramics are confirmed by X-ray powder diffraction (XRD, Rigaku, D/Max2500, Tokyo, Japan). To confirm the distortion of the BO_6 octahedron in the ceramics via a Raman spectrometer (RENISHAW inVia) using the 532 nm line from an Ar^+ laser. The microstructures of the samples are examined using a scanning electron microscope (SEM, S-3400N, Hitachi, Japan). A micro-electrometer (Keithley 6517B, Keithley, USA) is used to measure the resistivity of the ceramics as a function of temperature. X-ray photoemission spectroscopy (XPS, Thermo Fisher Scientific K-Alpha) is used to analyze the oxygen vacancy concentration. A piezoelectric force microscope (PFM, MFP-3D, USA) is used to study the domain structure. A precision impedance analyzer (TH2827, Tonghui Electronic Co, China) is used to measure the temperature dependence of the dielectric constant (ε_r) and electromechanical coupling factor (k_p). The nanoindentation method is employed to evaluate the hardness behaviors of KNNT-BNZ-BFO/*x* LiF ceramics at different doping contents. The ferroelectric TF Analyzer 2000 (aixACCT, Germany) is used to characterize the current (*I*-*E*) loops, the polarization *vs*. the electric field (*P*-*E*) behaviors, and the unipolar and bipolar strain *vs*. the electric field (*S*-*E*) loops. A quasi-static d_{33} meter (ZJ-3A, Institute of Acoustics, Chinese Academy of Sciences) is used for the piezoelectric coefficient (d_{33}) measurement of the ceramics. The *in-situ* temperature dependence of d_{33} is carried out by using a high-temperature piezometer (TZQD-D33T, China).

Results and discussion

Table S1 The crystal structure parameters and phase structure information of two phases of ceramics from the Rietveld structure refinement results.

x	0.002		0.004		0.006		0.010	
Sig	1.76		1.75		1.62		1.67	
R_w (%)	4.58		4.64		4.35		4.40	
Phase content (%)	R (38.24)	T (61.76)	R (35.91)	T (64.09)	R (38.09)	T (61.91)	R (34.86)	T (65.14)

a (Å)	3.9749	3.9718	3.9752	3.9726	3.9731	3.9709	3.9729	3.9715
b (Å)	3.9749	3.9718	3.9752	3.9726	3.9731	3.9709	3.9729	3.9715
c (Å)	3.9749	4.0131	3.9752	4.0134	3.9731	4.0126	3.9729	4.0145
$\alpha = \beta = \gamma$ (°)	90.0886	90	90.0899	90	89.9205	90	89.9192	90

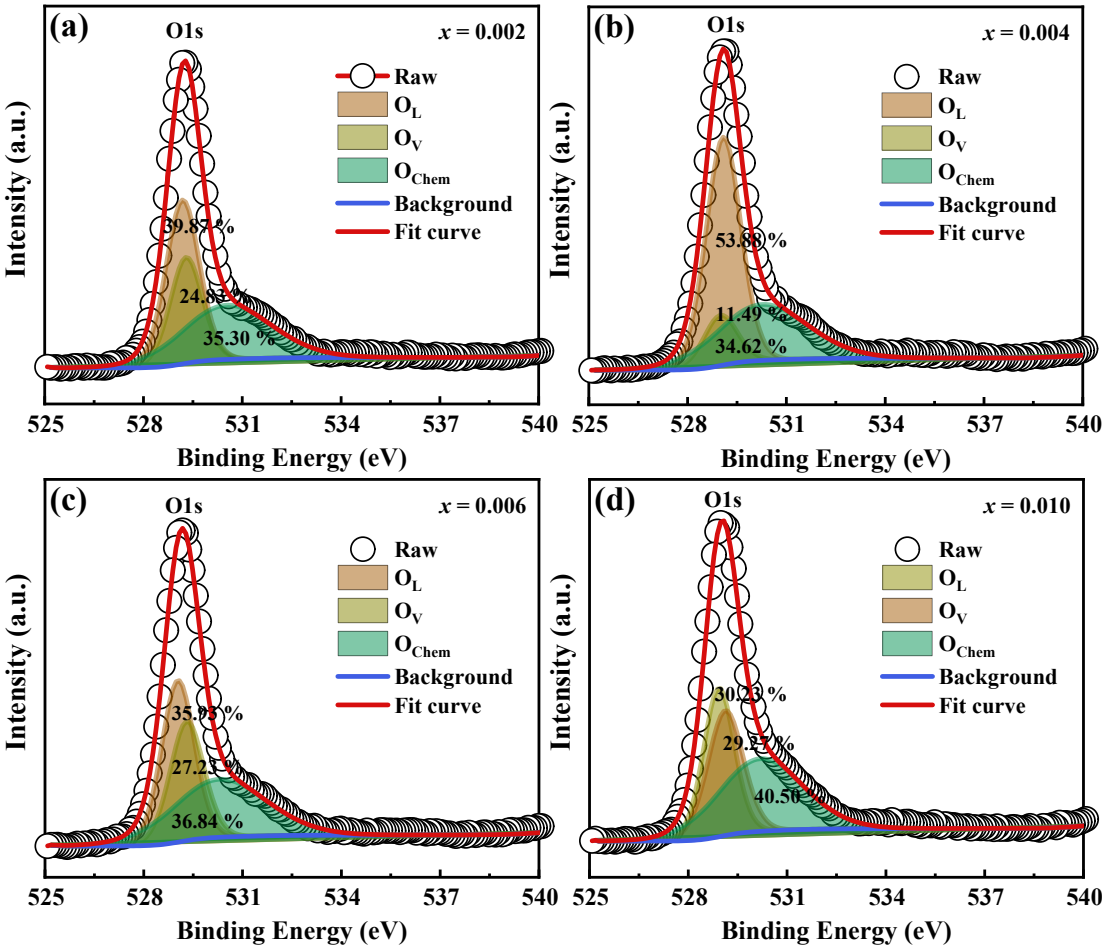

Fig. S1 (a-d) Fitting results for the O1s photoelectron spectra of the KNNT-BNZ-BFO/*x* LiF ceramics with (a) *x* = 0.002; (b) *x* = 0.004; (c) *x* = 0.006; (d) *x* = 0.010.

The temperature-dependent dielectric properties of the KNNT-BNZ-BFO/*x* LiF ceramics are analyzed using a modified Curie-Weiss law[1-3], as shown in Fig. S2(a)-(d). The diffuse-phase transition behavior of perovskite ferroelectrics can be expressed using this law, which relates the dielectric constant (ε) to temperature (T) and a constant (C). The modified Curie-Weiss law is shown in Equation (1).

$$\varepsilon = C/(T - T_0), \quad (1)$$

$$\Delta T_m = T_{cw} - T_m, \quad (2)$$

$$\frac{1}{\varepsilon_r} - \frac{1}{\varepsilon_m} = \frac{(T - T_m)^\gamma}{C} \quad (3)$$

The change in diffuse phase transition behavior of the ceramics is evaluated using the values of ΔT_m and diffuseness index (γ)[4]. ΔT_m is the difference between the transition temperature (T_m) and the Curie-Weiss temperature (T_{cw}), as shown in Equation (2). The γ is calculated using Equation (3), which relates the dielectric constants at the maximum (ε_m) and the transition (ε_r) temperatures to the temperature and the constant (C). Fig. S2(e) shows the $\log(\frac{1}{\varepsilon_r} - \frac{1}{\varepsilon_m})$ as a function of $\log(T\text{-}T_m)$ curves, which can be used to evaluate the diffuseness of the ceramics. The values of ΔT_m and γ first decrease and then slightly increase with an increasing x, indicating a change in the diffuse phase transition behavior. The improvement in ΔT_m and γ for the KNNT-BNZ-BFO/0.004 LiF ceramic is mainly due to the enhanced polarity resulting from the higher electronegativity of F ion compared to that of O ion[5]. These results suggest that the addition of a moderate amount of LiF can improve the local stress field and localized structural distortions of the ceramics. This improvement in the structural properties of the ceramics leads to changes in their diffuse phase transition behavior, as observed in the temperature-dependent dielectric properties.

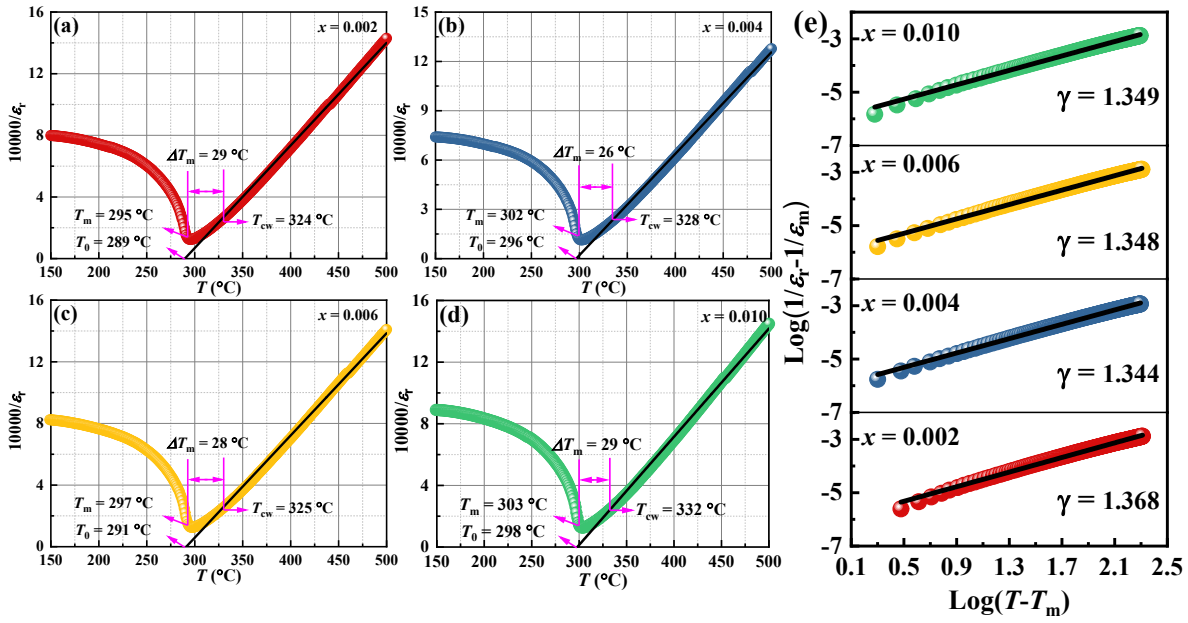

Fig. S2 (a)-(d) The relationship of the temperature and inverse dielectric permittivity of ceramics; (e) a plot of $\log(\frac{1}{\varepsilon_r} - \frac{1}{\varepsilon_m})$ as a function of $\log(T\text{-}T_m)$ for ceramics.

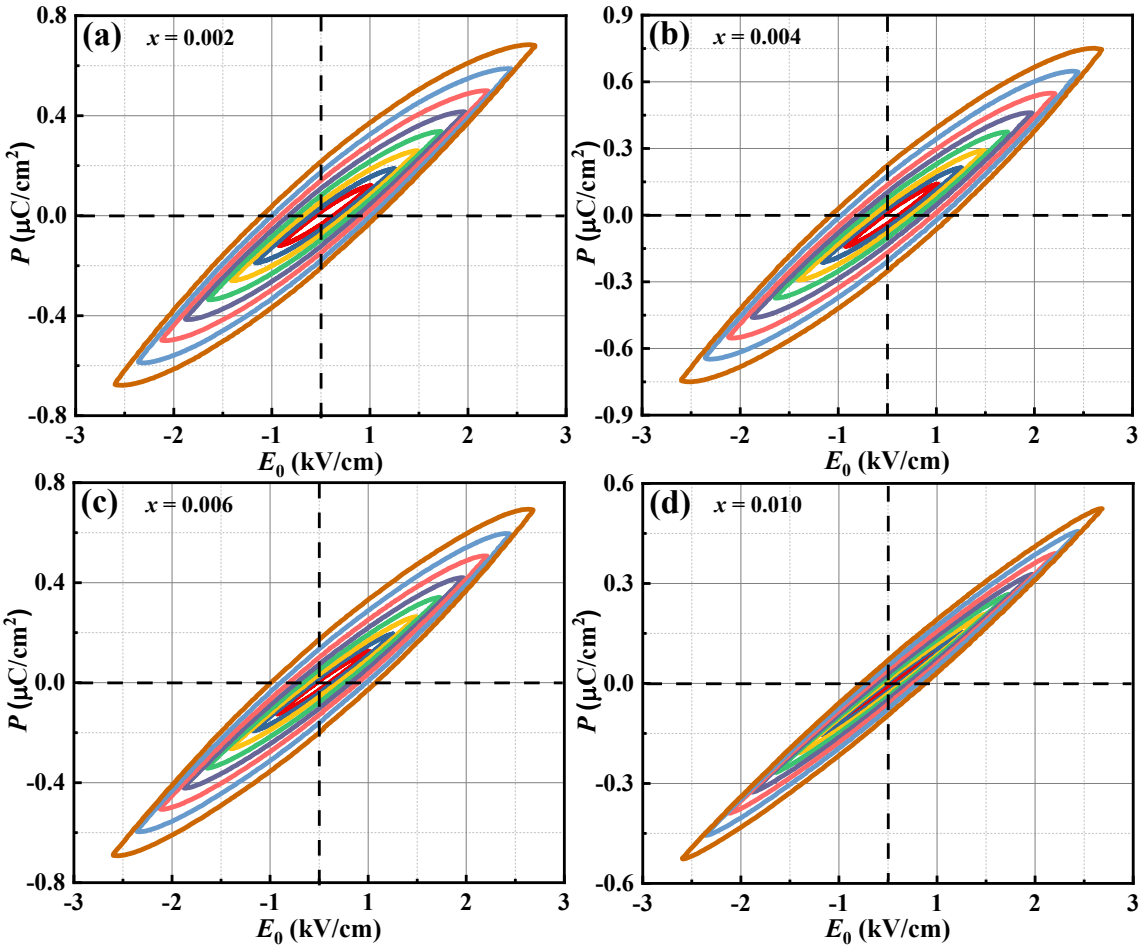

Fig. S3 (a)-(d) shows typical *P*-*E* curves in the sub-coercive field region for the KNNT-BNZ-

BFO/x LiF ceramics with (a) x = 0.002; (b) x = 0.004; (c) x = 0.006; (d) x = 0.010.

References

1. J. Xing, S. Xie, B. Wu, Z. Tan, L. Jiang, L. Xie, Y. Cheng, J. Wu, D. Xiao and J. Zhu, *Scripta Materialia*, 2020, 177 186-191.
2. J. Xing, Z. Tan, L. Xie, L. Jiang, J. Yuan, Q. Chen, J. Wu, W. Zhang, D. Xiao and J. Zhu, *Journal of the American Ceramic Society*, 2018, 101, 1632-1645.
3. M.-H. Zhang, Q. Zhang, T.-T. Yu, G. Li, H.-C. Thong, L.-Y. Peng, L. Liu, J. Ma, Y. Shen, Z. Shen, J. Daniels, L. Gu, B. Han, L.-Q. Chen, J.-F. Li, F. Li and K. Wang, *Materials Today*, 2021, 46, 44-53.
4. X. Ren, Z. Peng, B. Chen, Q. Shi, X. Qiao, D. Wu, G. Li, L. Jin, Z. Yang and X. Chao, *Journal of the European Ceramic Society*, 2020, 40, 2331-2337.
5. H. Tao, J. Yin, W. Wu, L. Zhao, J. Ma and B. Wu, *Journal of the American Ceramic Society*, 2022, 105, 5003-5010.